

IUE OBSERVATIONS OF SEYFERT GALAXIES¹

Chi-Chao Wu

Astronomy Dept., Computer Sciences Corporation

A. Boggess and T. R. Gull

Laboratory for Astronomy and Solar Physics

Goddard Space Flight Center

In this presentation we wish to discuss the following three topics:

- $L\alpha / H\beta$ ratio
- Continuous energy distribution
- Line profile

THE $L\alpha / H\beta$ RATIO

If the broad hydrogen lines in Seyfert galaxies and QSOs were produced by photoionization - recombination plus a small contribution from collisional excitation, the $L\alpha / H\beta$ ratio would be about 40. However, the composite spectrum derived by combining ground observations of high and low redshift QSOs shows $L\alpha / H\beta \sim 3$ (1). This result has subsequently been confirmed for a few individual QSOs such as 3C 273(2), PKS 0237-23(3) and B2 1225+31(4). With the IUE, it has become possible to measure the $L\alpha$ fluxes for a large number of Seyfert galaxies. Since the fluxes of Balmer lines are already available from ground-based observations, we can derive the $L\alpha / H\beta$ ratios for individual objects. In a recent paper (5) we presented the $L\alpha$ fluxes for 19 objects. Fifteen of these objects were observed by ourselves, and published data were used for the remaining four. The $L\alpha / H\beta$ ratios of type 1 Seyferts are also found to be about a factor of 10 lower than predicted by recombination theory. The results are summarized in Figure 1 where we plot the $L\alpha / H\beta$ ratio against the $H\alpha / H\beta$ ratio. Four reddening lines are also plotted in Figure 1. The origins of the reddening lines labeled A, B, C, and D correspond to $H\alpha / H\beta = 2.8$ and $L\alpha / H\beta = 40, 20, 10,$ and 5 respectively. The standard extinction curve of Code et al. (6) was used to construct the reddening lines. Increments of 0.1 in $E(B-V)$ are indicated by the tick marks along each reddening line. If simple recombination plus collision produce the emission in the broad line region (BLR) of Seyferts and QSOs, the observed points should concentrate at the origin of curve A; or, if there is dust along the line of sight, the observed points would lie along curve A. As indicated in Figure 1, there is no such concentration of points. In fact, the observed points do not cluster about any of the four reddening lines. Foreground reddening does not seem to play a major role in the low $L\alpha / H\beta$ ratio because, among the 19 objects, only I ZW 1, 3C 120, MKN 79 and NGC 7469 show

¹ Partially supported by a NASA research contract NAS 5-25774

reasonably strong 2200 \AA dust absorption features. On the average, these 4 objects do have higher $H\alpha / H\beta$ ratios than most others. Another interesting point in Figure 1 is that the objects having the largest $L\alpha / H\beta$ ratios are the type 2 Seyfert MKN 78 and the narrow line component of 3C 390.3. The broad component of 3C 390.3 has the low $L\alpha / H\beta$ ratio typical of type 1 Seyferts (7). It seems that the low $L\alpha / H\beta$ ratio is characteristic for the BLR and is probably caused by high density effects (see Ref. 8).

THE CONTINUOUS ENERGY DISTRIBUTION

In figure 2 we plot the continuous energy distribution of NGC 4151 and MKN 509 from the X-ray region to the infrared. Filled circles and triangles are observational data; solid and dashed lines are extrapolations. The X-ray fluxes are from the observations of Mushotzky et al. (9); the UV data (not corrected for reddening) are our own; the optical data are from de Bruyn and Sargent (10); and the IR data are from Rieke (11). For MKN 509 and some others, the spectrum may be turning over at $10.6 \mu\text{m}$. But from $3.6 \mu\text{m}$ to 1200 \AA , the data seem to indicate a single power law. The UV - IR power law is significantly steeper than the X-ray power law. This is true for 5 other Seyferts for which we have data from the X-rays to the UV and in a few cases to the IR. In some cases, the extrapolated optical (UV - IR) spectrum falls above the observed X-ray spectrum, suggesting a turnover in the UV, or alternatively a turn-up in the soft X-rays. This turnover may occur at about 1200 \AA as found by Green et al. (12) for quasars. Photons in the spectral region between the Lyman limit and the soft X-rays are the major source of heating for the emitting region, and Figure 2 makes it apparent that simple extrapolation of the optical spectrum may grossly overestimate the amount of energy available for heating.

Shields and Mushotzky (13) have studied the effect of hard X-rays on the emission lines of Seyfert galaxies and QSOs. They find that hard X-ray photons enhance the strength of high excitation lines. This result is confirmed by the UV spectra. Strong X-ray Seyferts like MKN 509, ESO 141-G55, and MCG 2-58-22 have $L\alpha / C\text{IV}$ ratios of about 2 or less, whereas UV spectra of weaker X-ray sources, like I Zw 1 and MKN 478, have $L\alpha / C\text{IV}$ ratio of about 5.

THE LINE PROFILE

The CIV 1550 line is relatively free of contamination by other emission lines, so it is suitable for line profile studies. In Figure 3, we have plotted the observed CIV line of MKN 509 (stepped line). Superimposed on the observed data are the computed profiles: 1. Gaussian (continuous curve); 2. Logarithmic (circles); and 3. The first exponential integral function (triangles). It is clear, in this case at least, that the Gaussian profile does not describe the observed data very well. At wavelengths not far from the line center, the logarithmic and the first exponential integral function profiles are essentially identical. In the far wings the first exponential integral function fits the data better. Capriotti, Foltz, and Byard (14, 15) have derived expected profiles of lines emitted by different kinematical and dynamical models of the BLR. They find

that logarithmic profiles can be produced by a spherical ensemble of discrete emitting clouds with steady state radial inflow or outflow. A ballistic radial outflow model produces profiles described by the first exponential integral function. As shown in Figure 3, the CIV $\lambda 1550$ profile of MKN 509 is best fitted by the first exponential integral function, indicating that the emitting clouds of the BLR are in ballistic outflow.

Our line profile fits were done independently for the blue portion and the red portion of the line. As indicated in Figure 3, when the blue side of the line (open circles) is reflected onto the red side, the red wing line profile (closed circles) is broader, in agreement with the Balmer line asymmetries found by Osterbrock (16). Capriotti, Foltz and Byard (11, 12) suggested that shielding of line photons by dust in the BLR or in the emitting clouds is the cause for this asymmetry. Anderson (17) on the other hand, proposed that the observed asymmetry is a result of gravitational redshift. Either mechanism could fit the asymmetry of the CIV profile.

REFERENCES

1. Baldwin, J. A. 1977, M. N. R. A. S., 178, 67p.
2. Boggess, A., et al. 1979, Ap. J., 230, L131.
3. Hyland, A. R., Becklin, E. E., and Neugebauer, G. 1978, Ap. J., 220, L73.
4. Soifer, B. T., Oke, J. B., Matthews, K., and Neugebauer, G. 1979.,
Ap. J., 227, L1.
5. Wu, C.-C., Boggess, A., and Gull, T. R., 1980, Ap. J., Nov. 15 issue.
6. Code, A. D., Davis, J., Bless, R. C., and Hanbury - Brown, R. 1976,
Ap. J., 203, 417.
7. Ferland, G. J., Rees, M. J., Longair, M. S., and Perryman, M. A. C.
1979, M. N. R. A. S., 187, 65p.
8. Kwan, J., and Krolik, J. H. 1979, Ap. J., 233, L91.
9. Mushotzky, R. F., Marshall, F. E., Boldt, E. A., Holt, S. S., and
Serlemitsos, P. J. 1980, Ap. J., 235, 377.
10. de Bruyn, A. G., and Sargent, W. L. W. 1978, A. J., 83, 1257.
11. Rieke, G. H. 1978, Ap. J., 226, 550.
12. Green, R. F., Pier, J. R., Schmidt, M., Estabrook, F. B., Lane,
A. L., and Wahlquist, H. D. 1980, preprint.
13. Shields, G. A., and Mushotzky, R. F. 1979, Astr. Ap., 79, 56.
14. Capriotti, E., Foltz, C., and Byard, P. 1980a, preprint.
15. . 1980b, preprint.
16. Osterbrock, D. E. 1977, Ap. J., 215, 733.
17. Anderson, K. S. 1980, preprint.

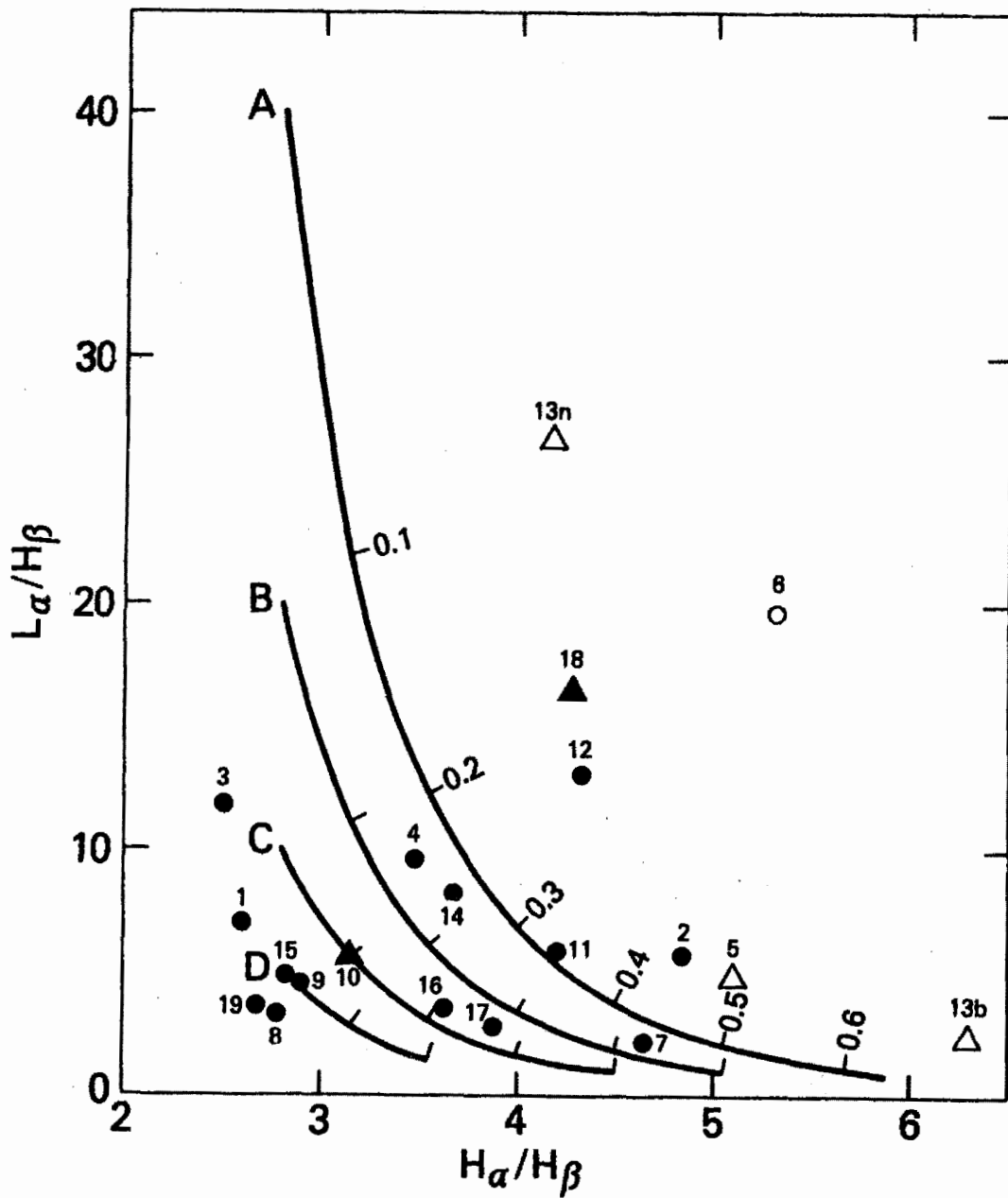


Fig. 1. The L_{α} / H_{β} - H_{α} / H_{β} diagram

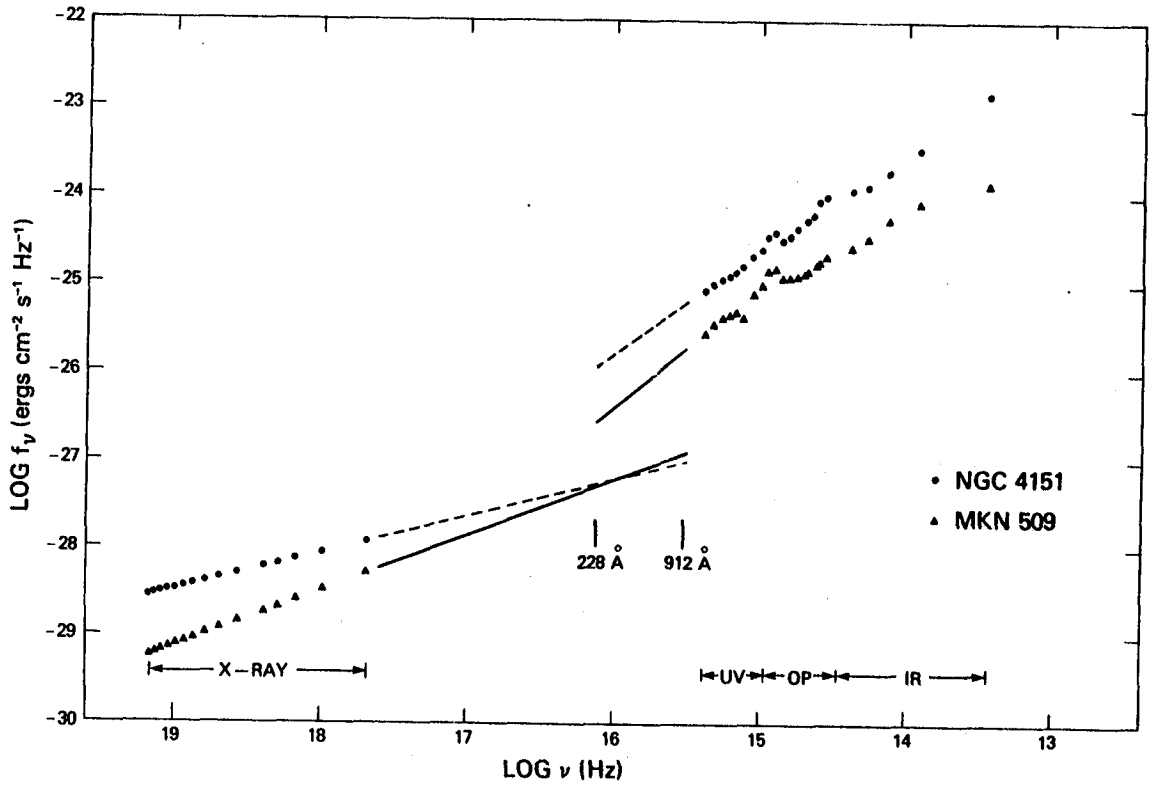


Fig. 2. The continuous energy distribution of Seyfert galaxies MKN 509 and NGC 4151.

MKN 509 C IV 1550 SWP 7330

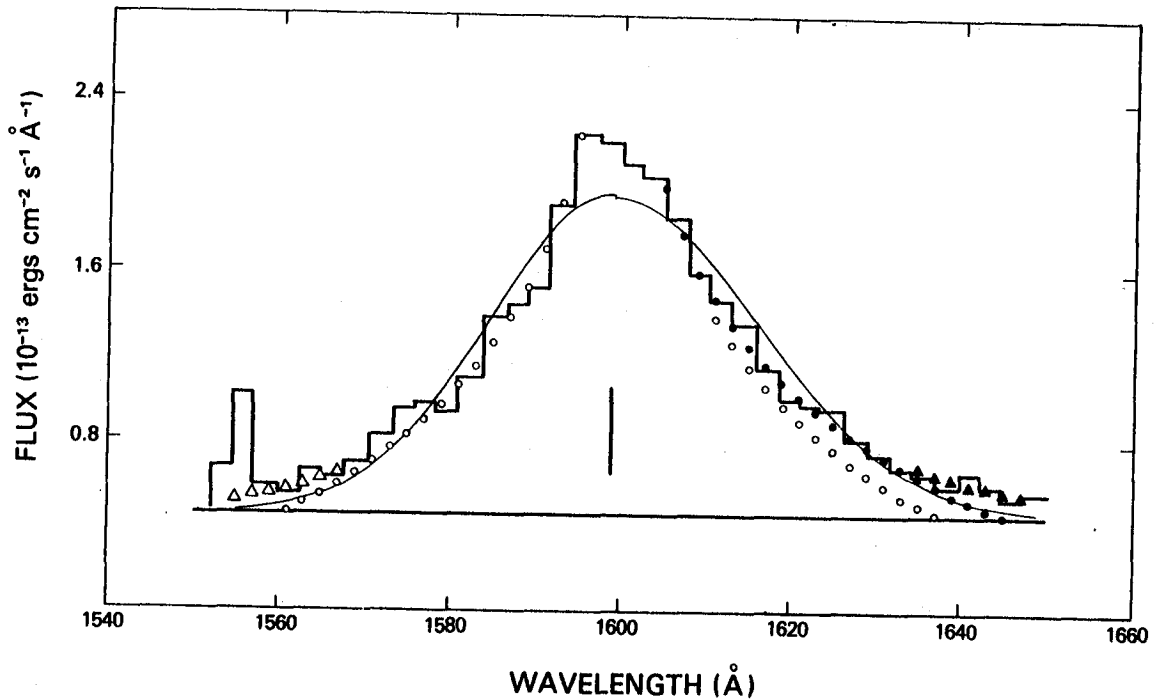


Fig. 3. The CIV $\lambda 1550$ line of MKN 509.